ACS NANO

www.acsnano.org

ARTICLE

Frequency-Upconversion Single-Mode Lasing in $CsPbBr_3$ Nanowires at Room Temperature

Junfeng Lu,* Long Yuan, Wenjie Deng, Xiaoxuan Wang, Tingcha Wei,* Changshun Wang, Zhi Zhang, Yanda Ji, Feifei Qin, Daning Shi, Caixia Kan, Chunxiang Xu,* and Caofeng Pan*

Cite This: https://doi.org/10.1021/acsnano.5c08513

Read Online

ACCESS | Metrics & More | Article Recommendations | Supporting Information

ABSTRACT: **Frequency upconversion provides a feasible strategy for switching the resonant wavelength of lasing modes. However, this nonlinear process requires extremely high optical properties for the medium. Here, the high-quality $CsPbBr_3$ nanowires were prepared by using the antisolvent method, which can serve as both the optical gain medium and resonant cavity. The highly polarized single-photon lasing was achieved with a low threshold of 6.69 $\mu J/cm^2$, excited by a 390 nm femtosecond pulse laser. Furthermore, frequency-upconversion single-mode lasing output was successfully operated at room temperature in a single $CsPbBr_3$ nanowire with a length of 3.5 μm under pumping of an 800 nm femtosecond pulse laser. These findings suggest that the prepared all-inorganic perovskite nanowires can be used as excellent optical gain media for frequency-upconversion lasers, providing a versatile platform for constructing nonlinear optoelectronic devices, such as optical switches, optical limiters, and biomedical imaging.**

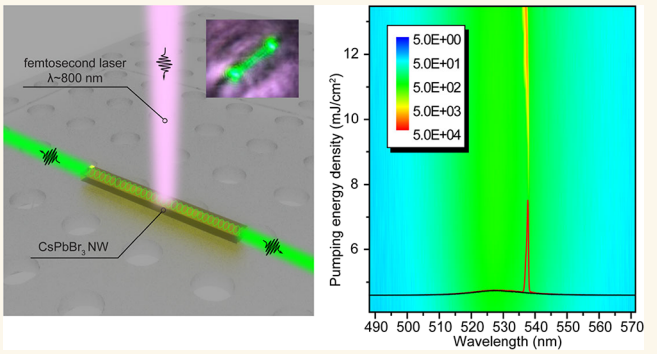

KEYWORDS: *frequency upconversion, single-mode lasing, low threshold, Fabry−Perot cavity, $CsPbBr_3$ nanowire*

1. INTRODUCTION

Nonlinear optics is an important branch of modern optics, which has been widely applied in fields such as laser technology, optical communication, and integrated optics.[1−3] Over decades, numerous nonlinear optical phenomena—including high-order optical harmonics, optical sum and difference frequencies, optical parametric amplification and oscillation, and multiphoton absorption and emission[4−7]—have been successively discovered. These discoveries have significantly advanced the development of laser modulation and ultrafast laser technology. Among them, two-photon emission, as a typical third-order nonlinear optical effect, has extensive applications in the fields of biomedical imaging,[8−11] optical data storage,[12] and sensing[13] due to many attractive merits over single-photon excitation processes, such as high spatial localization, long penetration depth, and low biological damage. Especially, the two-photon pumping technology at high power density provides a novel strategy for constructing frequency-upconversion lasers excited at red and near-infrared wavelengths without phase-matching requirements, which has been widely reported in traditional semiconductors.[14−19] However, this nonlinear optical process has extremely strict requirements for the optical gain and absorption efficiency of the dielectric medium.

Recently, all-inorganic perovskites, as emerging semiconductor materials, have attracted widespread attention in fields such as light-emitting diodes,[20,21] photodetectors,[22,23] and solar cells[24−26] due to their high fluorescence quantum efficiency, wide wavelength tunable range, long carrier lifetime, and long diffusion length compared with those of traditional semiconductors.[27−33] In particular, the two-photon absorption cross-section of up to 2.7 × 10^6 GM[34] and the near 100% fluorescence quantum efficiency[35] provide the necessary conditions for achieving frequency-upconversion laser emission. In addition, its relatively high exciton binding energy[36] and intrinsic self-absorption effect[37] have demonstrated unique advantages in constructing room-temperature single-mode lasers.[38−40] Moreover, the preparation methods of perovskite materials are flexible and diverse, which can not only serve as optical gain media but also provide natural resonant cavities for

Received: May 22, 2025
Revised: July 31, 2025
Accepted: July 31, 2025

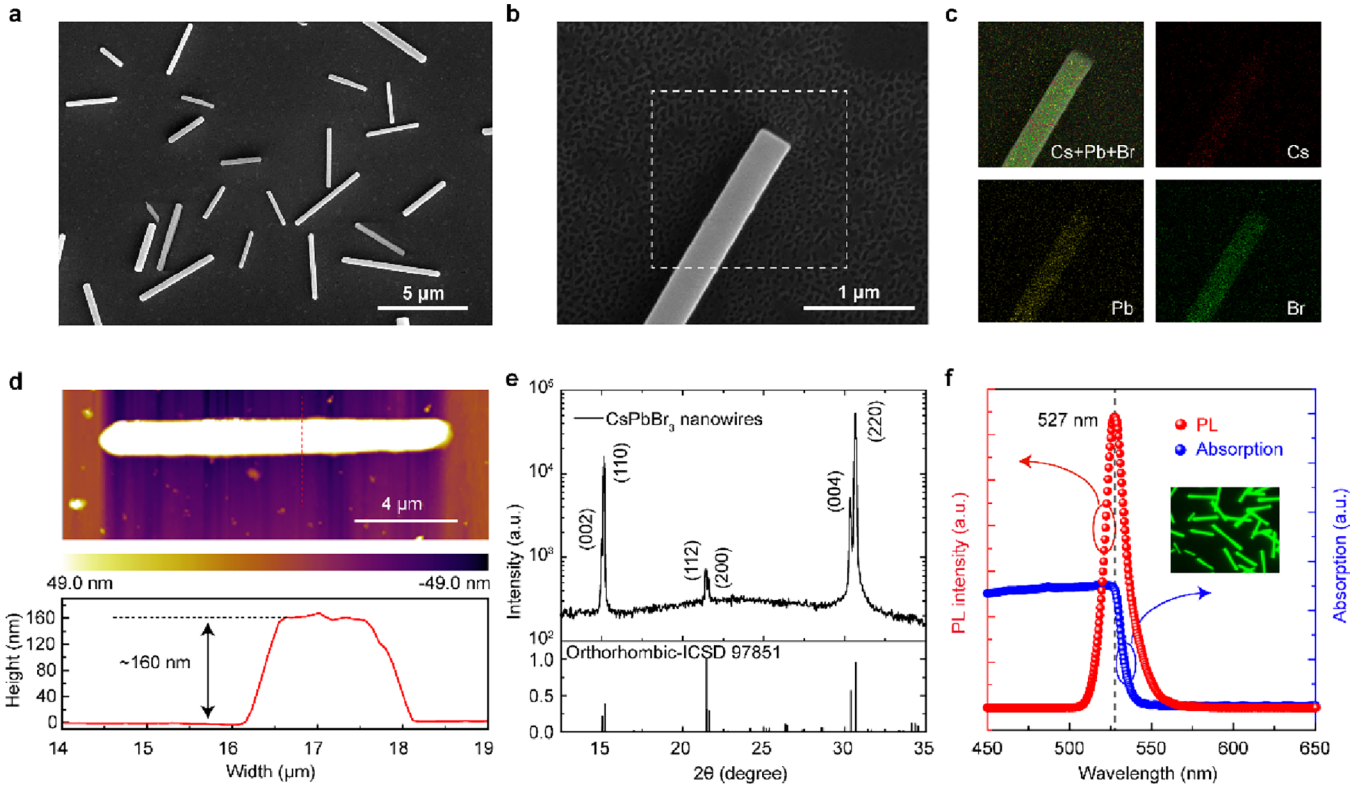

Figure 1. Characterization of morphology, structure, and optical performances for $CsPbBr_3$ nanowires. (a) Typical low-magnification scanning electron microscopy (SEM) image and (b) high-magnification SEM image of a single $CsPbBr_3$ nanowire. (c) Elemental mappings of Cs, Pb, and Br in nanowires; (d) atomic force microscopy (AFM) image and radial line scan curve of individual $CsPbBr_3$ nanowires; (e) X-ray diffraction pattern of $CsPbBr_3$ nanowires; and (f) photoluminescence (PL) and absorption spectra of $CsPbBr_3$ nanowires inserted with dark-field fluorescence imaging.

optical oscillation and mode selection, making them ideal materials for achieving frequency-upconversion lasers.

Herein, the antisolvent method was utilized to synthesize high-performance $CsPbBr_3$ nanowires as mentioned in our previous works,[41,42] where their two end faces serve as reflective mirrors to form an F−P resonator. The dominant factor for the broadening of temperature-related emission peaks was systematically analyzed through temperature-dependent PL spectra, and the exciton binding energy (31.2 meV) of perovskite materials was extracted to be slightly higher than the thermal ionization energy at room temperature (~26 meV). Subsequently, room-temperature frequency-upconversion single-mode lasing was successfully achieved in the classical FP resonant cavity of an individual $CsPbBr_3$ nanowire, excited by a femtosecond pulse laser with a wavelength of 800 nm.

2. RESULTS AND DISCUSSION

Figure 1a demonstrates a typical scanning electron microscopy (SEM) image of $CsPbBr_3$ nanowires prepared by the antisolvent method, with the lengths ranging from 2 to 20 μm and the widths ranging from 0.2 to 2 μm, uniformly distributed on a quartz substrate. The magnified close-up SEM image of the individual nanowire shown in Figure 1b indicates that its smooth surface and two uniform end faces can be used to construct a natural Fabry−Pérot (FP) cavity, where the latter serves as the two reflective mirrors of the resonator. Figure 1c exhibits energy-dispersive spectroscopy (EDS) mapping of Cs, Pb, and Br elements collected from the white dashed box in Figure 1b, indicating that each element is uniformly distributed on the nanowire. In addition, experiments using atomic force microscopy were performed to characterize the thickness of the $CsPbBr_3$ nanowires, which is approximately 160 nm, as shown in Figure 1d. Meanwhile, the obvious diffraction peaks located at 15.01°, 15.15°, 21.43°, 21.59°, 30.33°, and 30.67° can be assigned to the (002), (110), (112), (200), (004), and (220) crystal planes of orthorhombic perovskite-type $CsPbBr_3$ (space group *Pbnm*, a = 8.202 Å, b = 8.244 Å, c = 11.748 Å), corresponding to the standard card of ICSD 97851.[43] The splitting of diffraction peaks around 15° and 30° strongly suggests a distorted perovskite structure with tilted PbX_6 octahedra for the prepared $CsPbBr_3$ nanowires at room temperature. Furthermore, steady-state photoluminescence (PL), absorption, and fluorescence imaging measurements of perovskite nanowires were performed, as shown in Figure 1f. A remarkably strong spontaneous emission peak at 527 nm was observed at the absorption band edge, originating from intrinsic exciton radiative recombination. Large-area in situ fluorescence imaging of the perovskite nanowires (Figure S1, Supporting Information) demonstrates their excellent luminescence efficiency and uniformity, thus providing sufficient optical gain for light amplification.

In order to gain deeper insights into the optical properties of as-prepared $CsPbBr_3$ nanowires, measurements of temperature-dependent PL were performed with variable temperatures ranging from 93 to 293 K. Figure 2a shows the PL spectra as a function of temperature, exhibiting significant temperature dependence. As the temperature increases, the PL emission peak undergoes a slight blue shift with a difference of 2 meV, which mainly originates from the synergistic effect of

https://doi.org/10.1021/acsnano.5c08513
ACS Nano XXXX, XXX, XXX−XXX

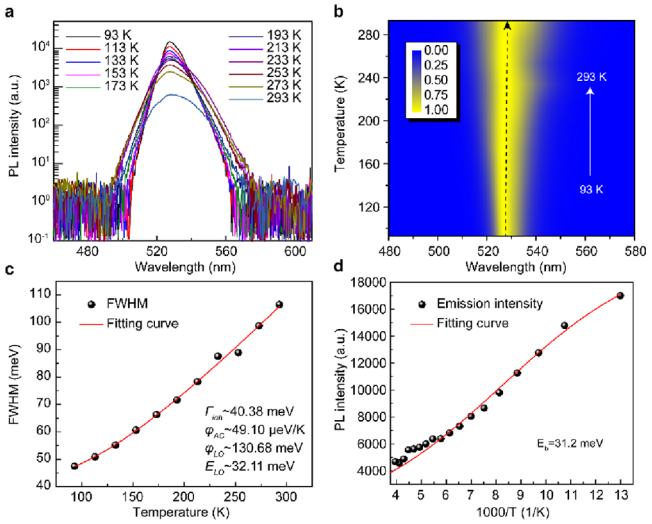

Figure 2. Temperature-dependent fluorescence characteristics of $CsPbBr_3$ nanowires. (a) PL spectra and (b) 2D pseudocolor plots of $CsPbBr_3$ nanowires at different temperatures from 90 to 293 K, and the dependence of (c) fwhm and (d) PL intensity on temperature.

band gap broadening induced by thermal expansion and electron−phonon coupling.[44,45] Interestingly, the full width at half-maximum (fwhm) of the PL emission peak is also accompanied by a broadening phenomenon. This is particularly evident and intuitive in 2D pseudocolor plots of normalized temperature-dependent PL spectra shown in Figure 2b. The temperature-dependent fwhm can be described by the sum of three broadening contribution terms given by Segall's expression,[46] as follows:

$$\Gamma(T) = \Gamma_{\text{inh}} + \varphi_{\text{AC}}T + \frac{\varphi_{\text{LO}}}{\exp(E_{\text{LO}}/k_{\text{b}}T) - 1} \quad (1)$$

where Γ_{inh} represents the temperature-independent inhomogeneity expansion constant caused by exciton−exciton interaction and crystal disorder. φ_{AC} is the exciton−acoustic phonon coupling coefficient, which is mainly determined by the temperature-dependent deformation potential interaction. φ_{LO} is the coupling coefficient of the exciton and longitudinal optical phonon, and E_{LO} is the longitudinal mode optical phonon energy. By fitting with Segall's expression, four parameters can be extracted as 40.38 meV, 49.10 μeV/K, 130.68 meV, and 32.11 meV, respectively, as shown in Figure 2c. The relatively small value of φ_{AC} suggests that linear exciton−phonon coupling makes almost no contribution to PL broadening. Therefore, the broadening of fwhm with increasing temperature mainly originates from the contribution of the exponential term of exciton−longitudinal optical phonon coupling. Moreover, an increase in temperature can give rise to a sharp decrease in PL emission intensity because of the thermally activated nonradiative recombination process, thus reducing the luminescence efficiency. Figure 2d shows the

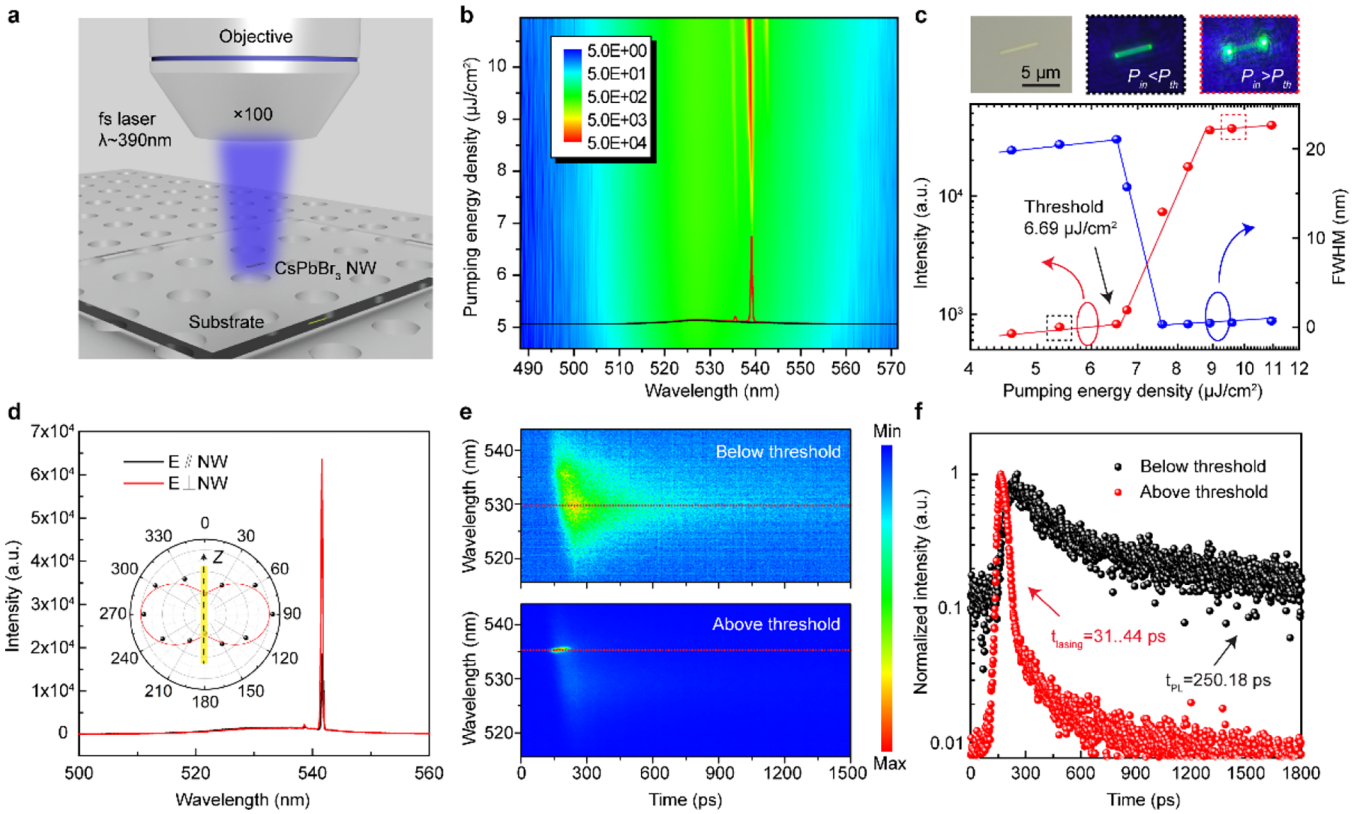

Figure 3. Single-photon pumped lasing characteristics of $CsPbBr_3$ nanowires. (a) Schematic diagram of $CsPbBr_3$ nanowires pumped by the μ-PL system; (b) 2D pseudocolor plots of lasing spectra for a single $CsPbBr_3$ NW with a length of 5.3 μm, excited by a 390 nm femtosecond laser; (c) dependence of emission intensity and fwhm on pumping energy density inserted with bright- and dark-field (below and above the lasing threshold ~ P_{th}) optical images; (d) emission polarization of the $CsPbBr_3$ NW laser; (e) temporal spectroscopic profiles; and (f) time-resolved PL spectra of $CsPbBr_3$ NW below and above P_{th}.

https://doi.org/10.1021/acsnano.5c08513
ACS Nano XXXX, XXX, XXX−XXX

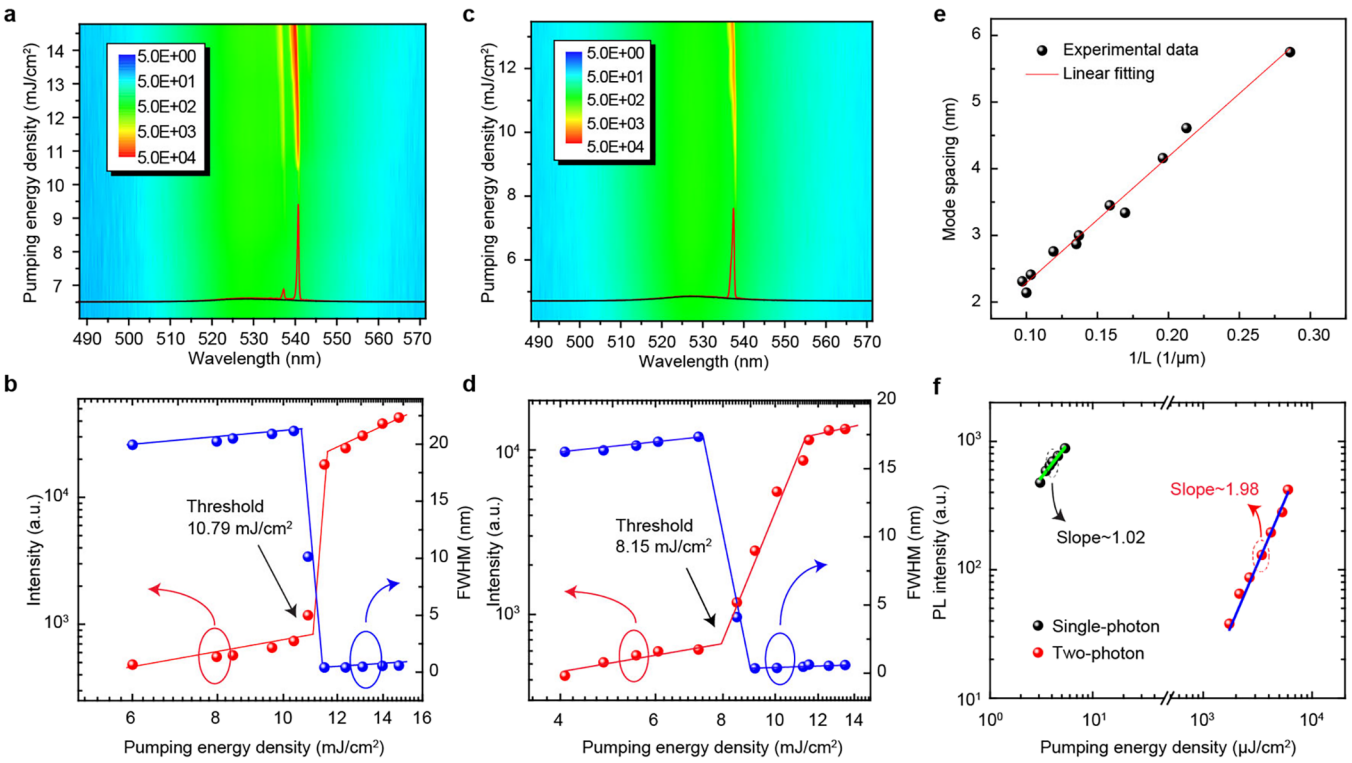

Figure 4. Frequency-upconversion lasing characteristics. 2D pseudocolor plots of lasing spectra for two $CsPbBr_3$ NWs with the length of (a) 6.3 μm and (c) 3.5 μm, respectively, excited by a 800 nm femtosecond laser; (b, d) dependence of emission intensity and fwhm on pumping energy densities for the corresponding $CsPbBr_3$ NWs; (e) mode spacing as a function of the reciprocal of cavity length (L); (f) dependence of PL intensity on pumping energy densities at the excited wavelengths of 390 and 800 nm fitting by a power exponential function.

dependence of PL intensity on the reciprocal of temperature, which can be analyzed by the Arrhenius equation as follows:[47]

$$I(T) = \frac{I_0}{(1 + Ae^{-E_b/k_bT})} \quad (2)$$

where I_0 represents the PL intensity at a temperature of 0 K. E_b is the exciton binding energy, which is extracted as 31.2 meV through fitting. It is slightly higher than the thermal ionization energy at room temperature (~26 meV), indicating that excitons can exist stably at room temperature. This is beneficial for constructing lasers operating at room temperature.

Figure 3a shows the schematic diagram of a single-photon pumped μ-PL system for a single $CsPbBr_3$ nanowire, which is excited by a 390 nm wavelength femtosecond pulse laser. The variable power emission spectra of a single $CsPbBr_3$ nanowire with a length of 5.3 μm were measured and plotted as 2D pseudocolor contour mapping, as shown in Figure 3b. It can be observed that the wide spontaneous emission transforms into the stimulated emission with an extremely narrow fwhm as the pumping energy density (P_{in}) gradually increases and exceeds 6.69 μJ/cm^2, accompanied by a sharp increase in emission intensity. It suggests that the prepared $CsPbBr_3$ has an extremely low lasing threshold of 6.69 μJ/cm^2, as shown in Figure 3c. Also, the phenomenon of stimulated emission can be confirmed by comparing the dark-field optical images as the nanowire is excited below and above the lasing threshold (P_{th}) shown in the inset of Figure 3c. When P_{in} is higher than P_{th}, the two ends of the nanowire emit the dazzling green lasing output with typical interference fringes, corresponding to the marked points in the red dashed rectangle frame. This indicates that the two end faces of the nanowire act as reflective mirrors, forming a classic Fabry–Pérot (FP) resonator and thereby generating lasing emission. Dark-field optical images of $CsPbBr_3$ nanowires with different sizes—excited above the lasing threshold (Figure S2, Supporting Information—all exhibited similar emission behavior. Moreover, the reduction in the size of the resonant cavity also leads to the evolution of the lasing mode structure, manifested by an increase in mode spacing and ultimately achieving single-mode lasing at a cavity length of 2.9 μm. In order to investigate the polarization characteristics of nanowire lasers, the emission spectra as a function of the detection polarization angle φ (referring to the long axis z of the nanowire) were measured, as shown in Figure 3d. The lasing peak exhibits highly polarized characteristics, where the intensity of the dominant lasing peak reaches its strongest (red solid line) when the detection polarization angle is 90° (i.e., perpendicular to the z-axis). The dependence of emission intensity on the detection polarization angle can be described by a $\cos^2\varphi$ function,[48] as shown in the inset of Figure 3d. The polarization degree of DOP = $(I_{max} - I_{min})/(I_{max} + I_{min})$ can be estimated to be 0.56. Also, the measurement of time-resolved PL (TRPL) spectroscopy (see Figure S3 in the Supporting Information) was performed to investigate the excitonic recombination dynamics behavior in excited nanowires. Figure 3e demonstrates the temporal spectroscopic profiles collected by a streak camera, as the pumping energy density is above and below the threshold. The TRPL spectra of these two states ($>P_{th}$ and $< P_{th}$), marked by the red dashed line, were extracted separately, as shown in Figure 3f. They can be fitted by a single-exponential decay function, and the extracted lifetimes are 250.18 ps for spontaneous emission and 31.44 ps for stimulated emission, fully suggesting the generation of stimulated amplification processes. In order to

https://doi.org/10.1021/acsnano.5c08513
ACS Nano XXXX, XXX, XXX−XXX

demonstrate that the nanowires that we grew have good stability at room temperature, we designed two stability testing experiments. One was a seven-day stability test on a single nanowire (see Figure S6a,b, Supporting Information). It can be seen that after the nanowire was placed at room temperature for 7 days, it still had stable laser output and remained in a single-mode state. We also conducted stability tests under continuous excitation using other nanowires (see Figure S6c–f, Supporting Information). It can be observed that after irradiating the nanowires with a laser for 20, 40, and 60 min, they still maintained relatively stable laser output and exhibited stable single-mode laser output. These two stability experiments fully demonstrated that the nanowires we grew possess excellent stability.

Subsequently, a femtosecond pulse laser with a wavelength of 800 nm was utilized to pump the $CsPbBr_3$ nanowires and investigate their two-photon pumped light emission behavior. Figure 4a shows the 2D pseudocolor plots of the lasing spectra of an individual nanowire with a length of 6.3 μm. As the pump energy density gradually increases and exceeds 10.79 mJ/cm^2, the intensity of the emission peak sharply increases, accompanied by a rapid narrowing of the fwhm, as shown in Figure 4b. In this case, the lasing threshold pumped by two photons is about 3−4 orders of magnitude higher than that of a single photon, indicating that the process pumped by two photons is more difficult due to its lower absorption efficiency compared to single-photon pumping. Furthermore, the lasing spectra (see Figure S4, Supporting Information) of the nanowires with different lengths were measured to analyze the evolution of their mode structures. Figure 4e shows the dependence of mode spacing on the reciprocal of cavity length L, exhibiting a typical linear relationship. This is in agreement with that given by the FP equation $\Delta\lambda = \lambda^2/2Ln_g$, where L represents the cavity length and n_g is the group refractive index. According to linear fitting, the group refractive index n_g can be extracted as 7.5 at around 535 nm, which is consistent with the results reported previously for lead bromide perovskite lasers.[49] As the length of the nanowire is further reduced to 3.5 μm, the intrinsic self-absorption effect and the limited optical gain region of the perovskite enable a two-photon pumped frequency-upconversion single-mode laser in this classical FP resonator, as shown in Figure 4c. Its side-mode suppression ratio (SMSR) and lasing quality (Q) factor were calculated to be 13.32 and 1450 dB (see Figure S5, Supporting Information), respectively. Our work has a much higher edge-mode suppression ratio compared to previous works and also has a higher Q factor. Moreover, while maintaining a high edge-mode suppression ratio and high Q factor, the laser threshold is at the same order of magnitude as those in other works, enabling a good balance of various performance aspects (Table 1, Supporting Information). The dependence of emission intensity and fwhm on pumping energy density shown in Figure 4d is similar to that of the longer nanowires mentioned above, indicating a transition from spontaneous emission to stimulated emission. Figure 4f compares the dependence of PL intensity on pumping energy density for single-photon and two-photon processes, both of which can be fitted by a power exponential function of $I \propto p^{\gamma}$. The power exponents γ of both are 1.02 and 1.98, respectively, further confirming the dominant role of two-photon absorption pumped by a low-energy 800 nm femtosecond pulse laser.

3. CONCLUSIONS

In summary, we systematically characterized the optical properties of $CsPbBr_3$ nanowires prepared by the antisolvent method through temperature-dependent PL spectroscopy, where the broadening of fwhm mainly originates from the coupling between excitons and longitudinal optical phonons. The higher exciton binding energy of 31.2 meV suggests that the $CsPbBr_3$ nanowire can be used to construct lasers operating at room temperature. Subsequently, single-photon-pumped lasing output with a polarization degree of 0.56 was achieved under the femtosecond pulse laser pumping at a wavelength of 390 nm, with a threshold of 6.69 μJ/cm^2, where the shortened lifetime from 250.18 to 31.44 ps indicates the transition from spontaneous emission to stimulated emission. Meanwhile, room-temperature frequency-upconversion single-mode lasing based on the FP oscillation mode was achieved in a $CsPbBr_3$ nanowire with a length of 3.5 μm by utilizing its intrinsic self-absorption effect. These results indicate the extensive application prospects of all-inorganic lead halide perovskite nanowires in constructing high-quality frequency-upconversion coherent nanosources.

4. EXPERIMENTAL SECTION

4.1. Preparation of $CsPbBr_3$ Nanowires. High-quality nanowires were synthesized through the antisolvent method. First, the precursor solution was prepared by dissolving CsBr and $PbBr_2$ powder (Alfa Aesar, 99.999%) with a molar ratio of 1:1 in anhydrous dimethylformamide (DMF) and stirring at 45 °C for 24 h. Subsequently, 30 μL of the precursor solution was dropped onto a quartz substrate and placed in a glass dish containing 30 μL of toluene as an antisolvent. Finally, the glass dish was placed in an oven with a setting temperature of 30 °C and reacted continuously for 24 h to obtain high-quality $CsPbBr_3$ nanowires.

4.2. Characterization of Morphology, Structure, and Optical Properties. The morphology and elemental analysis of nanowires were characterized by field emission scanning electron microscopy (FESEM, FEI Nova NanoSEM 450), equipped with an energy-dispersive spectrometer (EDS), and atomic force microscopy (AFM, Quantum Design). Their structural characteristics were measured through X-ray diffraction spectroscopy (XRD, D/MAX-2400). The measurements of steady-state photoluminescence (PL), absorption, and fluorescence imaging were performed through a highly integrated self-made micro system, consisting of a microscope (×50), a spectrometer, and a 3D displacement stage. The temperature was controlled by a cryogenic system (Linkam, HFS600E-PB2), covering a range of 77 K to room temperature. The lasing characteristics were measured by a confocal μ-PL system equipped with a wavelength-tunable femtosecond laser (190 fs, 6 kHz), an upright microscope, and an optical multichannel spectrometer (150/600/1800 g/mm). The signal of time-resolved PL was collected by a streak camera (Optoscope SC-10), equipped with an optical multichannel spectrometer (150/600/1800 g/mm) and a femtosecond laser system (100 fs, 1000 Hz), with an excitation wavelength of 325 nm.

ASSOCIATED CONTENT

Supporting Information

The Supporting Information is available free of charge at https://pubs.acs.org/doi/10.1021/acsnano.5c08513.

Bright-field and dark-field PL fluorescence imaging, lasing spectra and imaging for $CsPbBr_3$ nanowires with different lengths, temporal spectroscopic profiles of a single $CsPbBr_3$ nanowire, and two-photon pumped lasing spectra of $CsPbBr_3$ nanowires with different lengths (PDF)

https://doi.org/10.1021/acsnano.5c08513
ACS Nano XXXX, XXX, XXX−XXX

AUTHOR INFORMATION

Corresponding Authors

Junfeng Lu − *College of Physics, Nanjing University of Aeronautics and Astronautics, Nanjing 211106, PR China; Key Laboratory of Aerospace Information Materials and Physics (NUAA), MIIT, Nanjing 211106, PR China;* orcid.org/0000-0001-6458-7734; Email: lujunfeng@nuaa.edu.cn

Tingcha Wei − *School of Physics, South China Normal University, Guangzhou 510006, PR China;* Email: weitingcha@m.scnu.edu.cn

Chunxiang Xu − *State Key Laboratory of Bioelectronics, School of Biological Science and Medical Engineering, Southeast University, Nanjing 210096, PR China;* orcid.org/0000-0001-8116-2869; Email: xcxseu@seu.edu.cn

Caofeng Pan − *Institute of Atomic Manufacturing, Beihang University, Beijing 100191, PR China;* orcid.org/0000-0001-6327-9692; Email: pancaofeng@buaa.edu.cn

Authors

Long Yuan − *College of Physics, Nanjing University of Aeronautics and Astronautics, Nanjing 211106, PR China; Key Laboratory of Aerospace Information Materials and Physics (NUAA), MIIT, Nanjing 211106, PR China; Institute of Atomic Manufacturing, Beihang University, Beijing 100191, PR China*

Wenjie Deng − *College of Physics, Nanjing University of Aeronautics and Astronautics, Nanjing 211106, PR China; Key Laboratory of Aerospace Information Materials and Physics (NUAA), MIIT, Nanjing 211106, PR China*

Xiaoxuan Wang − *State Key Laboratory of Bioelectronics, School of Biological Science and Medical Engineering, Southeast University, Nanjing 210096, PR China*

Changshun Wang − *College of Physics, Nanjing University of Aeronautics and Astronautics, Nanjing 211106, PR China; Key Laboratory of Aerospace Information Materials and Physics (NUAA), MIIT, Nanjing 211106, PR China;* orcid.org/0000-0002-5288-4691

Zhi Zhang − *College of Physics, Nanjing University of Aeronautics and Astronautics, Nanjing 211106, PR China; Key Laboratory of Aerospace Information Materials and Physics (NUAA), MIIT, Nanjing 211106, PR China*

Yanda Ji − *College of Physics, Nanjing University of Aeronautics and Astronautics, Nanjing 211106, PR China; Key Laboratory of Aerospace Information Materials and Physics (NUAA), MIIT, Nanjing 211106, PR China*

Feifei Qin − *Peter Grünberg Research Centre, Nanjing University of Posts and Telecommunications, Nanjing 210003, P R China;* orcid.org/0000-0002-3947-7709

Daning Shi − *College of Physics, Nanjing University of Aeronautics and Astronautics, Nanjing 211106, PR China; Key Laboratory of Aerospace Information Materials and Physics (NUAA), MIIT, Nanjing 211106, PR China*

Caixia Kan − *College of Physics, Nanjing University of Aeronautics and Astronautics, Nanjing 211106, PR China; Key Laboratory of Aerospace Information Materials and Physics (NUAA), MIIT, Nanjing 211106, PR China;* orcid.org/0000-0003-3722-422X

Complete contact information is available at: https://pubs.acs.org/10.1021/acsnano.5c08513

Author Contributions

J.F.L., L.Y., and W.J.D. contributed equally to this work. Conceptualization: J.F.L. and L.Y.; methodology: L.Y., W.J.D., X.X.W., T.C.W., and C.S.W.; investigation: L.Y., Z.Z., Y.D.J. F.F.Q., D.N.S., and C.X.K.; data visualization: J.F.L., L.Y.; writing—original draft: J.F.L.; supervision: C.X.X. and C.F.P.

Notes

The authors declare no competing financial interest.

ACKNOWLEDGMENTS

The authors thank the support of the Natural Science Foundation of Jiangsu Province (BK20231441), the Fundamental Research Funds for the Central Universities (No. NS2024063), the Nanjing University of Aeronautics and Astronautics Graduate Student Research and Practice Innovation Program (xcxjh20232108, xcxjh20232101), the National Natural Science Foundation of China (Nos. 61805015, 52202099), and the Open Fund of the National Key Laboratory of Solid Microstructure Physics, Nanjing University (M38042).

REFERENCES

(1) Fernandez-Bravo, A.; Wang, D.; Barnard, E. S.; Teitelboim, A.; Tajon, C.; Guan, J.; Schatz, G. C.; Cohen, B. E.; Chan, E. M.; Schuck, P. J.; Odom, T. W. Ultralow-threshold, continuous-wave upconverting lasing from subwavelength plasmons. *Nat. Mater.* **2019**, *18* (11), 1172−1176.

(2) Rakher, M. T.; Ma, L.; Slattery, O.; Tang, X.; Srinivasan, K. Quantum transduction of telecommunications-band single photons from a quantum dot by frequency upconversion. *Nat. Photonics* **2010**, *4* (11), 786−791.

(3) Ferrera, M.; Razzari, L.; Duchesne, D.; Morandotti, R.; Yang, Z.; Liscidini, M.; Sipe, J. E.; Chu, S.; Little, B. E.; Moss, D. J. Low-power continuous-wave nonlinear optics in doped silica glass integrated waveguide structures. *Nat. Photonics* **2008**, *2* (12), 737−740.

(4) Terhune, R. W.; Maker, P. D.; Savage, C. M. Optical Harmonic Generation in Calcite. *Phys. Rev. Lett.* **1962**, *8* (10), 404−406.

(5) Armstrong, J. A.; Bloembergen, N.; Ducuing, J.; Pershan, P. S. Interactions between Light Waves in a Nonlinear Dielectric. *Phys. Rev.* **1962**, *127* (6), 1918−1939.

(6) Kroll, N. M. Parametric Amplification in Spatially Extended Media and Application to the Design of Tuneable Oscillators at Optical Frequencies. *Phys. Rev.* **1962**, *127* (4), 1207−1211.

(7) Kaiser, W.; Garrett, C. G. B. Two-Photon Two-Photon Excitation in CaF2: Eu2+. *Phys. Rev. Lett.* **1961**, *7* (6), 229−231.

(8) Denk, W.; Strickler, J. H.; Webb, W. W. Two-Photon Laser Scanning Fluorescence Microscopy. *Science* **1990**, *248* (4951), 73−76.

(9) Helmchen, F.; Denk, W. Deep tissue two-photon microscopy. *Nat. Methods* **2005**, *2* (12), 932−940.

(10) Yong, K.-T.; Qian, J.; Roy, I.; Lee, H. H.; Bergey, E. J.; Tramposch, K. M.; He, S.; Swihart, M. T.; Maitra, A.; Prasad, P. N. Quantum Rod Bioconjugates as Targeted Probes for Confocal and Two-Photon Fluorescence Imaging of Cancer Cells. *Nano Lett.* **2007**, *7* (3), 761−765.

(11) Olivier, N.; Luengo-Oroz, M. A.; Duloquin, L.; Faure, E.; Savy, T.; Veilleux, I.; Solinas, X.; Débarre, D.; Bourgine, P.; Santos, A.; Peyriéras, N.; Beaurepaire, E. Cell Lineage Reconstruction of Early Zebrafish Embryos Using Label-Free Nonlinear Microscopy. *Science* **2010**, *329* (5994), 967−971.

(12) Cumpston, B. H.; Ananthavel, S. P.; Barlow, S.; Dyer, D. L.; Ehrlich, J. E.; Erskine, L. L.; Heikal, A. A.; Kuebler, S. M.; Lee, I. Y. S.; McCord-Maughon, D.; Qin, J.; Röckel, H.; Rumi, M.; Wu, X.-L.; Marder, S. R.; Perry, J. W. Two-photon polymerization initiators for three-dimensional optical data storage and microfabrication. *Nature* **1999**, *398* (6722), 51−54.

(13) Pond, S. J. K.; Tsutsumi, O.; Rumi, M.; Kwon, O.; Zojer, E.; Brédas, J.-L.; Marder, S. R.; Perry, J. W. Metal-Ion Sensing Fluorophores with Large Two-Photon Absorption Cross Sections: Aza-Crown Ether Substituted Donor−Acceptor−Donor Distyrylbenzenes. *J. Am. Chem. Soc.* **2004**, *126* (30), 9291−9306.
(14) Lu, J.; Li, F.; Ma, W.; Hu, J.; Peng, Y.; Yang, Z.; Chen, Q.; Xu, C.; Pan, C.; Wang, Z. L. Two Photon-Pumped Whispering-Gallery Mode Lasing and Dynamic Regulation. *Adv. Sci.* **2019**, *6* (22), No. 1900916.
(15) Zhu, G. P.; Xu, C. X.; Zhu, J.; Lv, C. G.; Cui, Y. P. Two-photon excited whispering-gallery mode ultraviolet laser from an individual ZnO microneedle. *Appl. Phys. Lett.* **2009**, *94* (5), No. 051106.
(16) Yang, X. H.; Hays, J. M.; Shan, W.; Song, J. J.; Cantwell, E. Two-photon pumped blue lasing in bulk ZnSe and ZnSSe. *Appl. Phys. Lett.* **1993**, *62* (10), 1071−1073.
(17) Zhang, L.; Wang, K.; Liu, Z.; Yang, G.; Shen, G.; Lu, P. Two-photon pumped lasing in a single CdS microwire. *Appl. Phys. Lett.* **2013**, *102* (21), 211915.
(18) Landau, N.; Panna, D.; Brodbeck, S.; Schneider, C.; Höfling, S.; Hayat, A. Two-photon pumped exciton-polariton condensation. *Optica* **2022**, *9* (12), 1347−1352.
(19) Xing, G.; Liao, Y.; Wu, X.; Chakrabortty, S.; Liu, X.; Yeow, E. K. L.; Chan, Y.; Sum, T. C. Ultralow-Threshold Two-Photon Pumped Amplified Spontaneous Emission and Lasing from Seeded CdSe/CdS Nanorod Heterostructures. *ACS Nano* **2012**, *6* (12), 10835−10844.
(20) Lin, K.; Xing, J.; Quan, L. N.; de Arquer, F. P. G.; Gong, X.; Lu, J.; Xie, L.; Zhao, W.; Zhang, D.; Yan, C.; Li, W.; Liu, X.; Lu, Y.; Kirman, J.; Sargent, E. H.; Xiong, Q.; Wei, Z. Perovskite light-emitting diodes with external quantum efficiency exceeding 20%. *Nature* **2018**, *562* (7726), 245−248.
(21) Chen, J.; Wang, J.; Xu, X.; Li, J.; Song, J.; Lan, S.; Liu, S.; Cai, B.; Han, B.; Precht, J. T.; Ginger, D.; Zeng, H. Efficient and bright white light-emitting diodes based on single-layer heterophase halide perovskites. *Nat. Photonics* **2021**, *15* (3), 238−244.
(22) Shen, K.; Xu, H.; Li, X.; Guo, J.; Sathasivam, S.; Wang, M.; Ren, A.; Choy, K. L.; Parkin, I. P.; Guo, Z.; Wu, J. Flexible and Self-Powered Photodetector Arrays Based on All-Inorganic $CsPbBr_3$ Quantum Dots. *Adv. Mater.* **2020**, *32* (22), No. 2000004.
(23) Kang, C. H.; Dursun, I.; Liu, G.; Sinatra, L.; Sun, X.; Kong, M.; Pan, J.; Maity, P.; Ooi, E.-N.; Ng, T. K.; Mohammed, O. F.; Bakr, O. M.; Ooi, B. S. High-speed colour-converting photodetector with all-inorganic CsPbBr 3 perovskite nanocrystals for ultraviolet light communication. *Light Sci. Appl.* **2019**, *8* (1), 94.
(24) Chu, X.; Ye, Q.; Wang, Z.; Zhang, C.; Ma, F.; Qu, Z.; Zhao, Y.; Yin, Z.; Deng, H.-X.; Zhang, X.; You, J. Surface in situ reconstruction of inorganic perovskite films enabling long carrier lifetimes and solar cells with 21% efficiency. *Nature Energy* **2023**, *8* (4), 372−380.
(25) Akkerman, Q. A.; Gandini, M.; Di Stasio, F.; Rastogi, P.; Palazon, F.; Bertoni, G.; Ball, J. M.; Prato, M.; Petrozza, A.; Manna, L. Strongly emissive perovskite nanocrystal inks for high-voltage solar cells. *Nat. Energy* **2016**, *2* (2), 16194.
(26) Sun, J.; Hua, Q.; Zhou, R.; Li, D.; Guo, W.; Li, X.; Hu, G.; Shan, C.; Meng, Q.; Dong, L.; Pan, C.; Wang, Z. L. Piezo-phototronic Effect Enhanced Efficient Flexible Perovskite Solar Cells. *ACS Nano* **2019**, *13* (4), 4507−4513.
(27) Zheng, Y.; Liu, T.; Wu, J.; Xu, T.; Wang, X.; Han, X.; Cui, H.; Xu, X.; Pan, C.; Li, X. Energy Conversion Analysis of Multilayered Triboelectric Nanogenerators for Synergistic Rain and Solar Energy Harvesting. *Adv. Mater.* **2022**, *34* (28), No. 2202238.
(28) Hu, G.; Zhou, R.; Yu, R.; Dong, L.; Pan, C.; Wang, Z. L. Piezotronic effect enhanced Schottky-contact ZnO micro/nanowire humidity sensors. *Nano Research* **2014**, *7* (7), 1083−1091.
(29) He, J.; Zhou, R.; Zhang, Y.; Gao, W.; Chen, T.; Mai, W.; Pan, C. Strain-Insensitive Self-Powered Tactile Sensor Arrays Based on Intrinsically Stretchable and Patternable Ultrathin Conformal Wrinkled Graphene-Elastomer Composite. *Adv. Funct. Mater.* **2022**, *32* (10), No. 2107281.
(30) Jin, L.; Tao, J.; Bao, R.; Sun, L.; Pan, C. Self-powered Real-time Movement Monitoring Sensor Using Triboelectric Nanogenerator Technology. *Sci. Rep.* **2017**, *7* (1), 10521.
(31) Pan, C.; Guo, W.; Dong, L.; Zhu, G.; Wang, Z. L. Optical Fiber-Based Core-Shell Coaxially Structured Hybrid Cells for Self-Powered Nanosystems. *Adv. Mater.* **2012**, *24* (25), 3356−3361.
(32) Li, X.; Chen, M.; Yu, R.; Zhang, T.; Song, D.; Liang, R.; Zhang, Q.; Cheng, S.; Dong, L.; Pan, A.; Wang, Z. L.; Zhu, J.; Pan, C. Enhancing Light Emission of ZnO-Nanofilm/Si-Micropillar Heterostructure Arrays by Piezo-Phototronic Effect. *Adv. Mater.* **2015**, *27* (30), 4447−4453.
(33) Zhou, K.; Xu, W.; Yu, Y.; Zhai, W.; Yuan, Z.; Dai, K.; Zheng, G.; Mi, L.; Pan, C.; Liu, C.; Shen, C. Tunable and Nacre-Mimetic Multifunctional Electronic Skins for Highly Stretchable Contact-Noncontact Sensing. *Small* **2021**, *17* (31), No. 2100542.
(34) Xu, Y.; Chen, Q.; Zhang, C.; Wang, R.; Wu, H.; Zhang, X.; Xing, G.; Yu, W. W.; Wang, X.; Zhang, Y.; Xiao, M. Two-Photon-Pumped Perovskite Semiconductor Nanocrystal Lasers. *J. Am. Chem. Soc.* **2016**, *138* (11), 3761−3768.
(35) Liu, M.; Wan, Q.; Wang, H.; Carulli, F.; Sun, X.; Zheng, W.; Kong, L.; Zhang, Q.; Zhang, C.; Zhang, Q.; Brovelli, S.; Li, L. Suppression of temperature quenching in perovskite nanocrystals for efficient and thermally stable light-emitting diodes. *Nat. Photonics* **2021**, *15* (5), 379−385.
(36) Zhang, Q.; Su, R.; Liu, X.; Xing, J.; Sum, T. C.; Xiong, Q. High-Quality Whispering-Gallery-Mode Lasing from Cesium Lead Halide Perovskite Nanoplatelets. *Adv. Funct. Mater.* **2016**, *26* (34), 6238−6245.
(37) Lu, J.; Zhang, C.; Li, F.; Wang, R.; Qin, F.; Zhu, G. Realizing single-mode lasing in all-inorganic CsPbBr 3 perovskite microwires using intrinsic self-absorption. *Appl. Phys. Lett.* **2022**, *120* (17), 171105.
(38) Tang, B.; Dong, H.; Sun, L.; Zheng, W.; Wang, Q.; Sun, F.; Jiang, X.; Pan, A.; Zhang, L. Single-Mode Lasers Based on Cesium Lead Halide Perovskite Submicron Spheres. *ACS Nano* **2017**, *11* (11), 10681−10688.
(39) Li, F.; Jiang, M.; Cheng, Y.; Zhang, Y.; Yang, Z.; Peng, Y.; Ma, W.; Chen, Q.; Wang, C.; Liu, K.; Wang, R.; Lu, J.; Pan, C. Single-mode lasing of CsPbBr 3 perovskite NWs enabled by the Vernier effect. *Nanoscale* **2021**, *13* (8), 4432−4438.
(40) Yang, Z.; Lu, J.; ZhuGe, M.; Cheng, Y.; Hu, J.; Li, F.; Qiao, S.; Zhang, Y.; Hu, G.; Yang, Q.; Peng, D.; Liu, K.; Pan, C. Controllable Growth of Aligned Monocrystalline CsPbBr 3 Microwire Arrays for Piezoelectric-Induced Dynamic Modulation of Single-Mode Lasing. *Adv. Mater.* **2019**, *31* (18), No. 1900647.
(41) Li, M.; Lu, J.; Wan, P.; Jiang, M.; Mo, Y.; Pan, C. An Ultrasensitive Perovskite Single-Model Plasmonic Strain Sensor Based on Piezoelectric Effect. *Adv. Funct. Mater.* **2024**, *34* (41), No. 2403840.
(42) Li, M.; Lu, J.; Wan, P.; Jiang, M.; Lin, F.; Wu, X.; Liu, X.; Pan, C. Piezoelectric-Effect Enhanced Perovskite Plasmonic Nanolasers. *Adv. Opt. Mater.* **2023**, *11* (7), No. 2202723.
(43) Zhong, Y.; Liao, K.; Du, W.; Zhu, J.; Shang, Q.; Zhou, F.; Wu, X.; Sui, X.; Shi, J.; Yue, S.; Wang, Q.; Zhang, Y.; Zhang, Q.; Hu, X.; Liu, X. Large-Scale Thin CsPbBr 3 Single-Crystal Film Grown on Sapphire via Chemical Vapor Deposition: Toward Laser Array Application. *ACS Nano* **2020**, *14* (11), 15605−15615.
(44) Yu, S.; Xu, J.; Shang, X.; Ma, E.; Lin, F.; Zheng, W.; Tu, D.; Li, R.; Chen, X. Unusual Temperature Dependence of Bandgap in 2D Inorganic Lead-Halide Perovskite Nanoplatelets. *Adv. Sci.* **2021**, *8* (19), No. 2100084.
(45) Saran, R.; Heuer-Jungemann, A.; Kanaras, A. G.; Curry, R. J. Giant Bandgap Renormalization and Exciton-Phonon Scattering in Perovskite Nanocrystals. *Adv. Opt. Mater.* **2017**, *5* (17), No. 1700231.
(46) Lee, J.; Koteles, E. S.; Vassell, M. O. Luminescence linewidths of excitons in GaAs quantum wells below 150 K. *Phys. Rev. B* **1986**, *33* (8), 5512−5516.
(47) Crane, M. J.; Jacoby, L. M.; Cohen, T. A.; Huang, Y.; Luscombe, C. K.; Gamelin, D. R. Coherent Spin Precession and

https://doi.org/10.1021/acsnano.5c08513
ACS Nano XXXX, XXX, XXX−XXX

Lifetime-Limited Spin Dephasing in CsPbBr 3 Perovskite Nanocrystals. *Nano Lett.* **2020**, *20* (12), 8626−8633.
(48) Zhu, H.; Fu, Y.; Meng, F.; Wu, X.; Gong, Z.; Ding, Q.; Gustafsson, M. V.; Trinh, M. T.; Jin, S.; Zhu, X. Y. Lead halide perovskite nanowire lasers with low lasing thresholds and high quality factors. *Nat. Mater.* **2015**, *14* (6), 636−642.
(49) Shang, Q.; Li, M.; Zhao, L.; Chen, D.; Zhang, S.; Chen, S.; Gao, P.; Shen, C.; Xing, J.; Xing, G.; Shen, B.; Liu, X.; Zhang, Q. Role of the Exciton-Polariton in a Continuous-Wave Optically Pumped CsPbBr 3 Perovskite Laser. *Nano Lett.* **2020**, *20* (9), 6636−6643.

https://doi.org/10.1021/acsnano.5c08513
ACS Nano XXXX, XXX, XXX−XXX